Unstable Shear Slip Failure and Seismic Potential Investigation Using DEM in Underground Mining

Xu Ma[1,2] · Ping Zhang[1]

Abstract

Perturbations arising from mining operations significantly affect the stability of rock masses, and the influences aggerates with the rapid increase of mining-operation depths during recent years. The subsurface structures with major discontinuities subject to seismic hazards resulted from the shear-slip behaviors of rock masses. In order to identify the shear-slip regime of discontinuities and calculate seismic moment and seismic energy involved with shear-slip behaviors, we use discrete element modeling to study the shear slip failure along discontinuities in an underground mine. The recorded characteristic and properties of sub-contacts in DEM provide a basis for computing and visualizing the temporal and spatial distribution of seismic moment and seismic energy with mining operations. We computed the seismic energy and seismic moment using the numerical modeling method and the analytic method. We compared the result of summing seismic energy and seismic moment from the subcontacts of numerical models and the result of the analytic method. We confirmed that this tool can be used in comparative analyses. We also found that seismic moment and seismic energy, associated with shear stress drop and shear displacement increase, accumulate in the vicinity of major discontinuities. Mining operations at a greater depth cause greater changes of seismic moment and seismic energy, leading to a higher risk of inducing seismic hazards. Quantifying seismic potential using discrete element modeling can greatly facilitate the investigation of instability of geological discontinuities and thereby can help estimate the potential of seismic hazards.

1 Introduction

It has been long known that mining operations inevitably disturb the virgin state of stress in rock mass and cause stress redistribution in the rocks. Seismic pulses are triggered once the rocks subject to stress approach or exceed the strength of rocks [1]. In tectonic earthquake studies, it is concluded that ruptures are suddenly caused along pre-existing faults or discontinuities in most circumstances [2]. As the free face of mining advances, rock masses surrounding excavations are stressed approaching their elastic limit, leading to the inelastic deformation of the rock masses when the elastic

limit is surpassed [3–6]. Discrete element modeling, adapted for emulating heterogeneity of rocks, has been proven to be a powerful tool for evaluating the stability of rock masses in mining [7–9]. Linking a static numerical model to seismicity usually needs to qualitatively compare the locations of stress concentrations with the spatial distribution of seismic events [10]. A study confirmed that analysis based on linear relationships between stress and seismicity is not reliable by merely examining the correlations between stress and seismicity [11]. Additionally, this study also pointed out that it is likely to recognize highly stressed zones by monitoring seismicity, whereas forecasting the potential for seismicity and rockburst is still challenging [11]. On the other hand, calculating seismic energy release associated with seismicity can assist to quantitatively ascertain the relationship between stress and seismicity. Heunis (1980) proposed using the spatial energy release rate (ERR) as an index to evaluate the rockburst potential in mining [12]. Mounting studies support that most mining-induced seismic events are related to geological discontinuities in the surrounding rock

✉ Xu Ma
xuma@vt.edu

1 Division of Mining and Geotechnical Engineering, Luleå University of Technology, 97187 Luleå, Sweden

2 State Key Laboratory of Earthquake Dynamics, Institute of Geology, China Earthquake Administration, Beijing, China

masses [13–16]. The important part of assessing the seismic hazards in mining operations is to investigate the mechanical response caused by these geological discontinuities. Examining the interaction of faults, accordingly, is crucial for seismic hazard assessment and mitigation in terms of static stress transfer in spatial and temporal scales with fault activities [17]. In the study of fault interactions, the term "joint" is defined as mechanical and geological discontinuities which intersect near-surface rock masses [18]. Weakness planes, gradually formed by these discontinuities and joints, have a good potential for inducing seismic events along with shear-slip behaviors of weakness planes, even if the mining-induced stress is lower than the threshold stress for fracture development in rock masses. Furthermore, production blasts appear to trigger and raise the risk of rockburst in the surrounding rock masses. Many researchers found that the shear-slip behavior along the weakness plane is linked to a sudden shear stress drop and a simultaneous shear displacement [19–23]. This characteristic can be used as a signature for the identification of the initiative of the shear slip behaviors in numerical simulations accordingly.

It is summarized that seismic events caused by high stresses are usually with lower magnitude and less damaging than fault-slip type events [24]. The classic Coulomb failure criterion was initially applied to assess the fault-slip potential in static stress fields. A fault-slip dislocation model was introduced to estimate the constant stress drop with near-source displacement during a fault slip and examine the correlation between the rupture size and the magnitude of seismic events [25]. Simpson (1986) concluded that the most direct characteristic of stress change is the abrupt release of stress during a seismic slip [26]. Regions with low-strength rock mass containing geological discontinuities are more likely to subject to stress release. Stress is accumulated until a threshold level, which usually approaches or exceeds the strength of the rock mass. A threshold is achieved to result in the yielding behavior with a seismic event and its stress drop in rock. This stress drop is followed by a recovery of shear stress until another seismic event appears. The seismic moment and the stress drop can be interpreted in terms of the strain energy release of seismicity. Despite the existence of analytic methods for shear energy calculation, quantifying the energy release during shear slip behavior is not reliable due to the complex motions in the system. Bormann and Giacomo (2010) pointed out that merely a limited portion of the total energy release transmits to generating seismic waves because the major portion needs to drive the growth of fracture and overcome the friction [2]. The lessons we learned about discrete element modeling as a tool for analyzing geomechanical response in mining can be well applied to quantifying seismic moment and seismic energy for shear slip behavior in rock masses. The DEM modeling allows for simulating large deformation of rock masses, especially for the shear behavior of joints. Integrating quantifications of the seismic moment and seismic energy into the shear slip behavior

characterization in numerical modeling can facilitate the identification and evaluation of potential seismic hazards. Gu and Ozbay (2014, 2015) used the 2D continuously yielding (CY) joint model to study the unstable shear failure of rock discontinuities in underground mining conditions [27, 28]. Zoheir and Ozbay (2018) presented a computational framework for studying both compressive-type rockburst and shear-type rockburst [29]. The 3D CY model study focusing on the mining field is limited. We developed the 3D CY model study associated with in situ mining conditions. Additionally, we employed the subcontact of the mesh in numerical modeling to compute the energy participation during the unstable shear slip.

Today's mining operations in Kiirunavaara Mine are within highly stressed regions at great depths, adding new complexities on top of the rock mass instability influenced by stress perturbation and geological discontinuities. Our study on a major discontinuity at a hard rock mine suggests that mining operations result in shear slip along the discontinuity in the surrounding regions. Seismic moment and seismic energy release associated with the shear slip behavior are recognized by summing each unit of the mesh network in a discrete element model. This study begins by exploring the capability of the continuously yielding (CY) joint model and examining whether it can be suitably applied to simulating shear slip behaviors of rock masses of Kiirunavaara Mine. Then, we point out methods of computing seismic moment and seismic energy and introduce how to integrate them using subcontacts of the CY joint model. We continue to construct the mine scale model, investigate mechanical responses of a series of monitoring points located on the joint, and examine the spatial distribution and evolution of seismic moment and seismic energy on the joint with consecutive removal of sublevel caving blocks. It is found that applying CY joint model in DEM models for underground mines can assist in accurately predicting unstable shear slip behavior along discontinuities of rock masses and providing insights into forecasting rockburst in fault-slip type.

2 Data and Methods

2.1 Geological Settings and Seismic Events

We firstly performed a direct shear test. Then, the result of the direct shear test is examined to validate the seismic moment and the seismic energy calculation using information from subcontacts of the joint. By summing the shear energy of all subcontacts and comparing the total amount of shear energy with the analytic result, we verify that subcontacts of the CY joint model are reliable for recording the shear energy evolution during the shear slip.

Kiirunavaara Mine is one of the world's largest underground mines. The mining method used in the mine is sublevel caving. Its orebody extends about 4000 m, strikes nearly north–south, and dips 55–60° toward the east (Fig. 1). The average width of the orebody is 80–100 m, and the total lateral extension of the orebody is more than 4 km. The main part of the orebody is fine-grained magnetite and fine-grained apatite. The footwall consists of trachyte and the hanging wall consists of rhyolite. The overall quality of the rock mass shows as strong and brittle [30]. The rock properties and material parameters are from a previous study [30], which obtained these parameters from lab tests. According to the geological investigations around blocks 30, 34, and 38 in levels 1079–1137 m, the rock mass within this block accommodates roughly 6500 major fractures/joints, which were broadly divided into multiple groups by their strike-dipping directions. It has been concluded by previous studies that the discontinuities parallel with the dip direction weaken the stability most during mining operations. This group of discontinuities is described as near-N-S to NW striking, dipping steeply (60–90°) to the east.
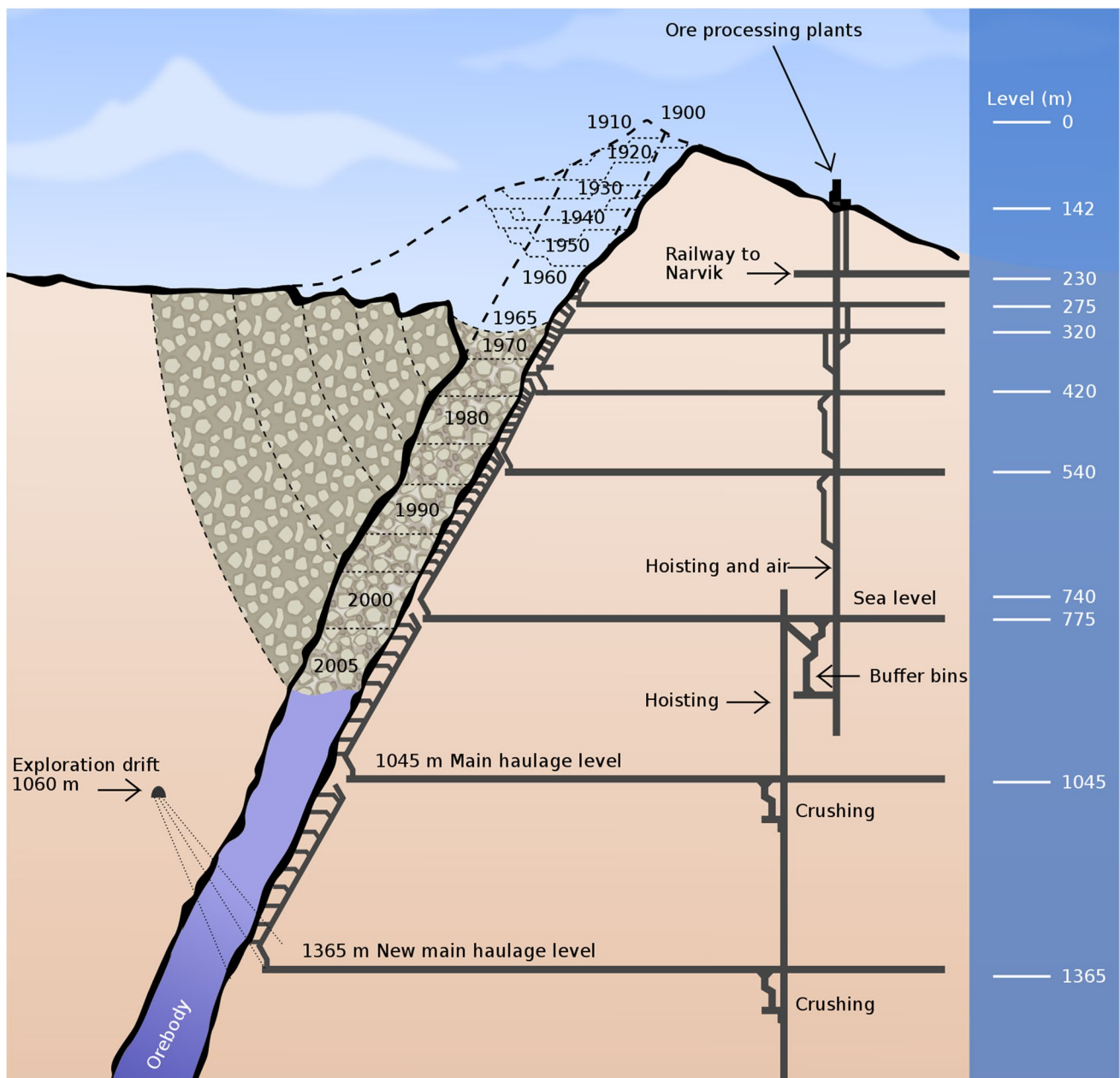

Fig. 1 Geological settings of Kiirunavaara Mine

The mine has been regarded as seismically active after it experienced several large seismically induced rock falls since 2007 [31]. More than 1000 seismic events per day have been recorded in the whole mine during recent years. Most of the damaging seismic events investigated in block 33/34 of the mine from 2008 to 2013 were categorized as fault-slip type. With the increasing depth of mining operations and involving complex geological discontinuities, it is anticipated that seismic activities will continue to be active in long term. Four fault/shear slip type event seismic events were captured from 2014 to 2016 (Table 1).

2.2 Unstable Shear Slip and CY Joint Model

Compared with tension joints, shear joints are usually marked as a shape of planar (Barton, 1973). Shear slip is caused when the resistance for the fault to slip is overcome by the shear stress posing on the slip surface. Mohr–Coulomb criterion can be used to evaluate the resistance. The fault slip seismic events are induced by unstable release of shear stress with slipping over a planar area, which is the plane of weakness in a rock mass. The signature associated with the occurrence of seismic events in fault slip type is the significant shear stress drop of sliding along shear surfaces. Fault slip seismic events often belong to the category of medium (Moment magnitude > 0) and large (moment magnitude > 1) events, while strain burst type events are usually less than medium magnitude. According to seismological studies, unstable slip along a plane is determined by factors including shear stress and frictions along the plane. Shear stress functions as a drive force to induce the seismic event. In contrast, the static friction and the shear strength of the plane constrain the shear activity along the plane. Ryder (1988) introduced the static friction τ_s using a direct shear test, which consists of two blocks of rocks with a mutual nearly smooth contacting interface [20]. It was found that frictional resistance to shear slip increases with the normal confining stress σ_n in a linear relationship,

$$\tau_s = c + \mu\sigma_n \tag{1}$$

where c represents cohesion, μ is the tanϕ means the coefficient of the static friction, and ϕ is the angle of static friction. As suggested in Byerlee's law, the cohesion c is close to 0 and μ ranges from 0.5 to 1.0.

The shear stress drop implies the appearance of violent shear instability [1]. Cook (1976) pointed out that unstable failure can only be described by considering that the rock fails in a brittle mode with sudden post-failure loss in strength. Previous studies proved that the CY joint model can capture post-peak behaviors of discontinuities by successfully targeting the evolution of shear strength for the joint with accounting for accumulated plastic displacement and incorporating it as a measure of damage [32, 33]. The continuously yielding model, accordingly, is capable of describing the unstable shear slip failure, which has been commonly observed on the residual behavior of rock joints. Compared with the Mohr–Coulomb plasticity model, the CY joint model begins displaying irreversible nonlinear behavior from the onset of the shear slip by considering joint shear and normal stiffness dependence of normal stress and nonlinear behavior in the post-peak regime [27]. As a result, the dilation angle in the CY joint model decreases as the accumulation of damage on the plane of weakness. The signature of unstable shear slip failure using the CY joint model is a shear stress drop and a synchronous, rapid shear displacement increase. Specifically, as CY joint model accounts for the dependence of joint shear and normal stiffness on non-linear hardening and softening behavior, it is capable of delineating the internal mechanisms of progressive shear damage of discontinuities.

A direct shear test using two rock blocks is performed to verify the shear stress drop with shear slip. The direct shear test validates the applicability of the CY joint model by incorporating related parameters of Kiirunavaara Mine, which are listed in Table 2. As shown in Fig. 2, block A is placed on top of block B, which was constrained on the ground. Block A is a block of cube shape with a side length of 0.2 m. Block B is a cuboid shape with a rectangular shape in the cross-section. The geometry of these two blocks is shown in Fig. 2. Block A is initially placed on the center of the top surface of block B. Normal stress of 30 MPa is applied on block A. A constant velocity of 0.001 m/s along the horizontal direction is applied on block A to exert shear loading on the contacting surface of the two blocks. The frictional surface between them is assigned with the CY joint model. The average shear stress and shear displacement of the frictional interface are monitored and computed. The

Table 1 Times, locations, and magnitude of large seismic events in Kiirunavaara Mine

Event	Date	Time	North (m)	East (m)	Depth (m)	Magnitude (M_L)	Seismic moment (Nm)	Seismic energy (J)
1	December 25, 2014	1:56	3387	6468	1012	2.0	1.6×10^{12}	1.0×10^7
2	September 17, 2015	13:30	2586	6343	1150	2.0	1.1×10^{12}	1.8×10^7
3	September 24, 2015	4:53	2948	6323	1097	2.0	1.1×10^{12}	1.2×10^7
4	May 22, 2016	2:31	3345	6408	1112	1.9	7.8×10^{11}	8.3×10^6

Table 2 Parameters used for the CY joint model in the direct shear test

Joint property	Unit	Value
Joint normal stiffness	GPa/m	110
Joint shear stiffness	GPa/m	90
Joint normal stiffness exponent	Not applicable	0
Joint shear stiffness exponent	Not applicable	0
Joint basic friction angle	°	30
Joint initial friction angle	°	65
Roughness parameter	mm	0.1

signature of shear slip along the horizontal plane between two blocks is a sudden shear stress drop (Fig. 2c) and a pronounced shear displacement increase (Fig. 2c). As shown in Fig. 2c, the shear stress reached the peak right before initiating the shear slip and then the shear stress turns to decrease, which implies the initiation of the shear slip along the horizontal plane. The shear stress continues to decrease until reaching a constant level of the shear stress. Before achieving this constant level of shear stress, the evolution of the shear stress versus the shear displacement notably fluctuates at a decreasing trend due to the friction effect on the slip surface (Fig. 2d).
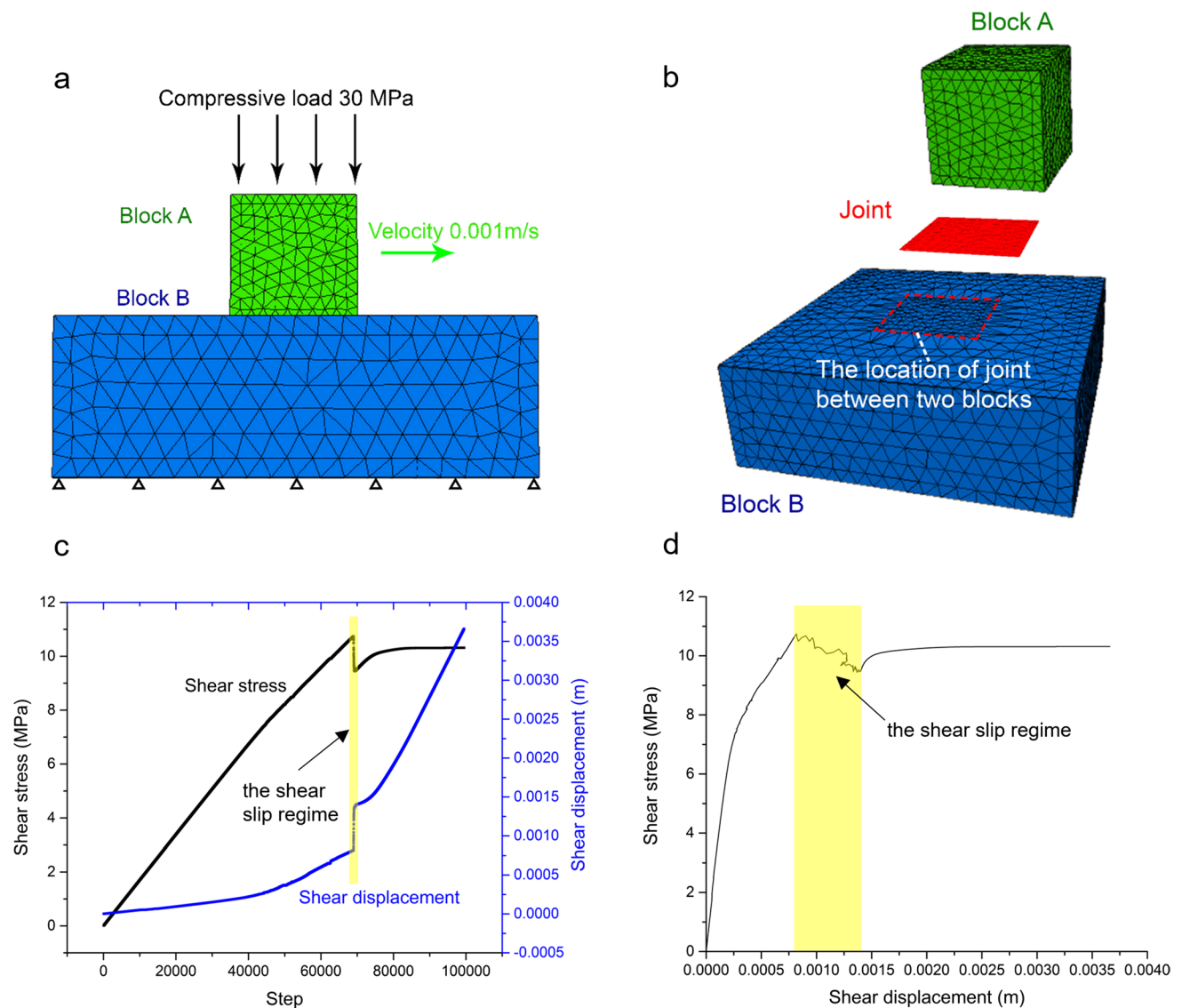
Fig. 2 The direct shear test setup and mechanical responses of the joint assigned with the CY joint model. **a** Longitudinal view of two blocks with boundary conditions and loading conditions. **b** Isometric view for the configuration of blocks and the joint. The evolution of the **c** average shear stress and average shear displacement, as well as **d** shear stress versus shear displacement of the joint between two blocks. The highlighted part in yellow color shows the evolution of shear stress versus shear displacement during the shear slip regime, which is also highlighted in **c**

The joint, assigned with the CY model a 3DEC model, is generated with an evenly distributed mesh network including triangle shapes before applying the constant velocity along the horizontal plane (Fig. 2a). After block A displaces at the constant velocity, some new submesh areas are automatically generated so that more subcontacts form in this joint (Fig. 2b). With the continuous loading of the constant velocity, the shear stress increases to overcome the friction of the joint surface and thereby causes a sudden shear slip along the joint plane. In this sudden shear slip, the shear displacement steeply increases, and the shear stress sharply decreases by a significant amount. The significant change in shear stress and shear displacement is considered as the signature of the shear slip behavior (Fig. 2c, d), which can be depicted by the CY joint model. By comparing the number of subcontacts of the mesh network at the moment right before the slip and that right after the slip, the area of the mesh after the shear slip appears to be larger than that before the shear slip (Fig. 3). The mesh network generates more subcontacts for adapting the shear slip motion along the joint plane, because the shear displacement suddenly increases due to the shear slip behavior along the joint plane.

We examine the record, including shear displacement, shear stress, and area of each subcontact, through the moment after the shear slip from the output of 3DEC. Using the difference of shear stress, shear displacement, and area of each subcontact between the moment of beginning shear slip and post shear slip, we compute the seismic moment and seismic energy release of this shear slip activity. The seismic energy, calculated using Eq. 6 on the values shown in Fig. 2c, is 1.46×10^{-5}. The seismic energy summed on all subcontacts is 1.58×10^{-5} J. The quantitative similarity of the seismic energy based on two calculation ways proves that it is viable to integrate subcontacts of the CY joint model for seismic potential.

After ensuring all time steps using the subcontact change to calculate the seismic moment and seismic energy, we apply the CY model to the mine scale model and further compute the seismic moment and shear energy change of the shear slip along discontinuities.

2.3 Seismic Moment and Seismic Energy Calculation

The concept of excess shear stress was introduced to evaluate whether seismic events of the fault slip type can be generated with the rupture. Excess shear stress is defined as the differential value when the shear stress overcomes the resistance (dynamic strength) of the weakness plane to initiate the shear slip:

$$\tau_e = |\tau| - \mu\sigma_n \tag{2}$$

where τ_e represents the excess shear stress, $|\tau|$ is the shear stress, μ means the coefficient of the static friction, and σ_n is the normal stress applied on the slip plane (Ryder 1988).

The seismic moment and the stress drop during an earthquake can be used to estimate strain energy release. The elastic strain energy contains two parts:

$$W = H + E \tag{3}$$

where $H = \sigma_f DS$ is the frictional loss, and E is the wave energy. σ_f is the frictional stress during shear slip along the fault [34]. The difference in the elastic strain energy W before and after a seismic event based on the elastic stress relaxation model is:

$$W = \sigma DS \tag{4}$$

where σ is the average stress during the form of fault, D is the average offset on the fault, and S is the area of the fault. Stress drop $\Delta\sigma$ is approximately equal to 2σ, if the stress drop is complete. Thus, there is:

$$W = W_o = 1/2\Delta\sigma DS = (\Delta\sigma/2\mu) \tag{5}$$

where $\mu = (3 \sim 6) \times 10^{11}$ for crust-upper mantle conditions. W_o is the minimum strain energy drop in the process of forming a seismic event.

Fig. 3 Mesh network distribution of the joint in the direct shear test **a** before the shear slip and **b** after the shear slip. The zoom-in area in **b** illustrates that new subcontacts are generated following the shear slip

a
Joint mesh network
before the shear slip

b
Joint mesh network
after the shear slip
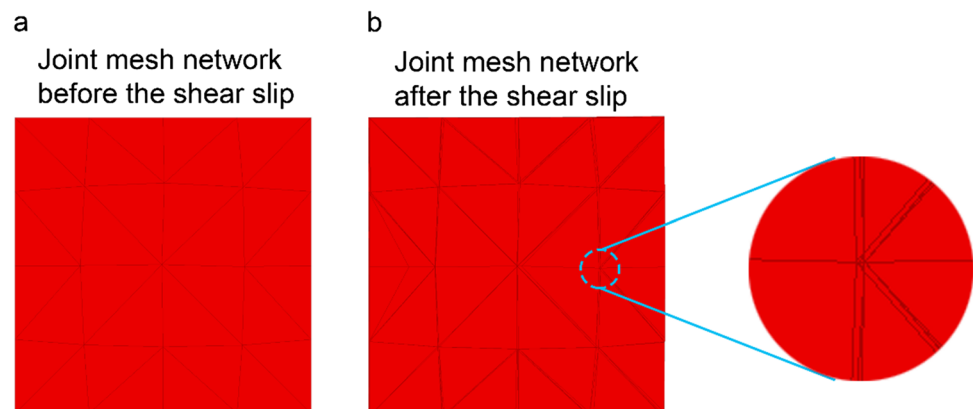
The seismic moment represents the amount of force needed to radiate seismic waves and is defined as:

$$M = \mu \times D \times A \tag{6}$$

where μ is the shear modulus for quantifying the rock rigidity. The product of $D \times A$ means the inelastic strain [34].

It has been long known that seismic energy release comes from the transformation of elastic strain to inelastic strain in the process of fracture propagation and frictional sliding. Seismic events aroused from this transformation can be divided into slow creep-like events and fast dynamic seismic events based on the average velocity of deformation at the seismic source. Slow type events, consequently, produce seismic waves with low frequency.

Given that the rupture energy is negligible, the seismic energy can be calculated by:

$$W_k = \frac{1}{2} \int \tau_e D dA \tag{7}$$

where τ_e is the excess shear stress drop, D is the slip distance along the rupture plane, and A represents the area of the rupture surface.

By combining the mathematical expression of the seismic moment and seismic energy, the average shear stress drop τ_{ae} is summarized by:

$$\tau_{ae} = 2\frac{W_k}{DA} = 2\frac{\mu W_k}{M} \tag{8}$$

where M is the seismic moment, and W_k is the seismic energy [34].

3 Results

The geometry of the mine scale model is shown in a longitudinal view (Fig. 4a) and an isometric view (Fig. 4b). The total lateral extension of the orebody is about 4 km with a thickness ranging from 0 to more than 200 m. With the increase of depth, the overburden stress is larger, which poses more effects. According to the geological structure mapping, a major discontinuity is extracted from a series of fracture sets with similar orientations. The simplified major joint is listed in Table 3. The major discontinuity, represented by a joint surface in the 3DEC model, is parallel to the interface between footwall and orebody and is placed 20 m away from this interface. The major joint used in the 3DEC model is simplified from the characteristics information of discontinuities depicted in the geological structure mapping of Kiirunavaara Mine. Blocks are the proxy for the hanging wall, orebody, and footwall. These blocks are separated by joints that represent the ore-footwall, ore-hanging-wall contacts, and discontinuities. Geological structure mapping shows that discontinuities in this category

Table 3 The discontinuity simulated in the 3DEC model

Major joint	Strike	Dip angle
1	0°	60°
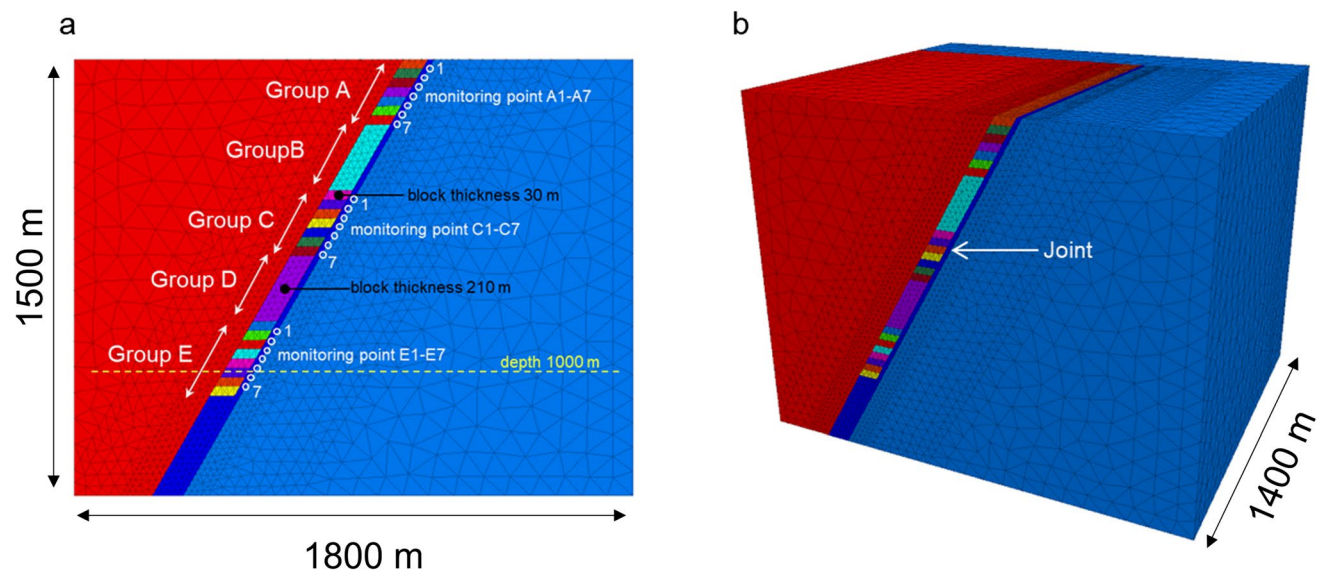
Fig. 4 The mine scale model in **a** longitudinal view and **b** isometric view in 3DEC for block layer excavation with observing monitoring points along the major joint for Kiirunavaara Mine. The main block in red color represents the hanging wall; the main block in blue color represents the footwall. We divide the excavated block into 5 groups: groups A, B, C, D, and E. Groups A, C, and E are divided into sub-blocks. The monitoring points are set up on the joint, and they are arranged along the main joint

of strike-dip are the most common ones. This group of discontinuities plays a critical role in seismicity, and therefore, seismic events of fault-slip type were very likely to be triggered adjacent to these discontinuities. This dominant group of discontinuities is near-E-W striking and is dipping intermediately steep, ranging from 50 to 80°, to the south. Fractures of this major group show typically relatively rough surfaces, and the thickness varies from a few millimeters to tens of centimeters.

This simplified joint that represented the group of discontinuities can simulate the shear slip behaviors along these discontinuities and facilitates the modeling and computing process using 3DEC. The orebody is divided into five groups marked from group A to group E with increasing depth. Among them, group A, group C, and group E are evenly subdivided into seven layers and the thickness of each layer is 30 m. Group B and group D are set up with 210 m thickness and are considered as contact blocks between other groups with subdivisions (groups A, C, E). All the layers are sequentially excavated from the top to the bottom of the orebody. For groups A, C, and E, a series of monitoring points is marked along the discontinuity and each monitoring point is located in the same depth of the lower border of each block layer. The mechanical responses of monitoring points are examined and recorded. After block excavations, which are emulated by removing horizontal layers, we continue to trace these monitoring points in the evolution of the shear stress and shear displacement. In addition, the records of subcontacts of the joint surface, including shear force, shear displacement, and the subcontact area, allow us to accurately compute seismic moment and seismic energy during mining operations that are mimicked by the excavation of horizontal block layers.

3.1 Parameters Applied in the Mine Scale Model

The parameters, shown in Tables 4 and 5, of footwall, hanging wall, orebody, and discontinuities are assigned to the corresponding blocks and the major joint of the mine scale model. The overall dimensions of the model are developed according to the in situ conditions of the Kiirunavaara Mine and are shown in Fig. 4. Production drifts and ore passes are not incorporated in the model for the simplicity fashion.

Table 4 Block parameters used in this study

	Density (kg/m^3)	Bulk modulus (GPa)	Shear modulus (GPa)
Footwall	2800	33	20
Orebody	4700	21	13
Hanging wall	2800	33	20

Table 5 Parameters for discontinuities used in the conceptual mine-scale models

Joint property	Unit	Value
Joint normal stiffness	GPa/m	50
Joint shear stiffness	GPa/m	50
Joint normal stiffness exponent	0	0
Joint shear stiffness exponent	0	0
Joint basic friction angle	°	30
Joint initial friction angle	°	65
Roughness parameter	mm	0.1

In this model, the depth ranges from the ground surface to 1700 m level, the range in east–west direction is set up as 1500 m, and the north–south direction spans 1800 m including three major blocks. Four side surfaces are constrained along directions that are perpendicular to these surfaces. The bottom surface is fixed at all directions. The top surface is applied with normal stress following Eq. (5). The in situ stresses applied in the numerical model are based on the equations proposed by Sandström (2003) and are listed in Eq. (5).

$$\sigma_x = 2.22 + 0.037z$$
$$\sigma_y = 1.74 + 0.029z \qquad (9)$$
$$\sigma_z = 1.68 + 0.028z$$

where z represents the depth below the ground surface, σ_x is the stress in the east–west direction, σ_y represents the stress in the north–south direction, and σ_z is the stress in the depth direction.

Gradient mesh is enabled and designed to ensure the trade-off of accuracy and computing efficiency. Regions surrounding the orebody and the major discontinuity use the most refined meshes for better capturing and reflecting the mechanical responses due to excavations. Coarser meshes are developed when the other regions are beyond a larger range.

3.2 Unstable Shear Slip Behavior Identification

The shear slip along the discontinuity is identified and depicted by the CY model. We select the block layers including the 4th, 5th, and 6th blocks that are located in the lower portion of the subdivided groups. We first compare the three neighboring block layers from the same group. Then, we pick the 4th block from each group and compare the mechanical responses across them.

To analyze the mechanical response of monitoring points affected by excavations, we pick three consecutive monitoring points A4, A5, and A6 from the 4th, 5th, and 6th excavation levels, respectively. The evolution of shear displacement

and shear stress with progressing excavations are examined (Fig. 5). As shown in Fig. 5, mp-A4 (the monitoring point A4) experiences a sudden increase of shear displacement and a pronounced stress decline after the excavation of the 5th block A5 in group A. The change of shear displacement and shear stress at mp-A5 appear to have a similar pattern after the excavation of the 5th block A5. The excavation of block A6 continues to induce a significant change of shear stress and shear displacement at mp-A5 so that the shear displacement increase and shear stress drop exhibit again after the excavation of block A6. Similarly, the excavation of the 6th block A6 triggers the increase of shear displacement and the reduction of shear stress at mp-A6 (the monitoring point A6). The signature of change of shear displacement and shear stress at these monitoring points indicate that the excavation of blocks directly affects the stability of the major joint in the footwall, leading to unstable shear slip along the major joint.

The mechanical response of other monitoring points including those near block group C and the ones in the vicinity of block group E are also examined. It is found that mp-C4 initially experiences the unstable shear slip following the excavation of block C4 (Fig. 6). In a similar manner, the monitoring point mp-C5 manifests that, caused by the excavation of block C5, the shear displacement abruptly rises and the shear stress decreases simultaneously (Fig. 6). This phenomenon implies that unstable shear slip occurs at this monitoring point. Furthermore, at the next level of depth, monitoring point mp-C6 appears with the same signature of unstable shear slip following the excavation of block C6 (E-C6).

In order to investigate the joint behavior at a larger depth, we continue examining the performance of monitoring points that are adjacent to block group E (Fig. 7). The expected unstable shear slip behavior is found at these monitoring points as well. For example, the monitoring point mp-E4 experiences the shear slip increase and shear stress drop after the excavation of block E4. The magnitude of the shear displacement change because the excavation of E4 is larger than that of the excavation of E3. The excavation of block E4 causes the other sudden shear stress reduction and corresponding shear displacement increase at the monitoring
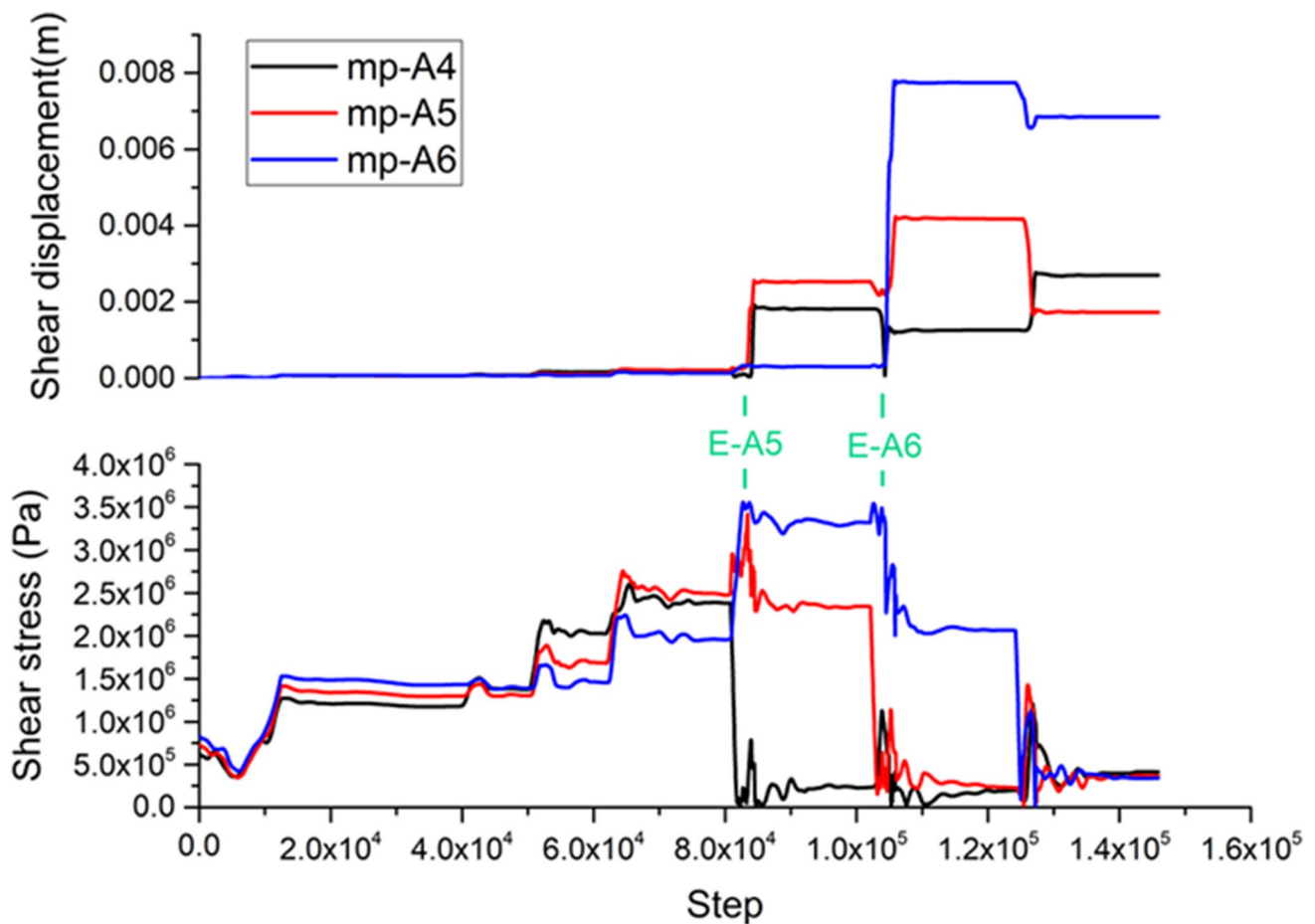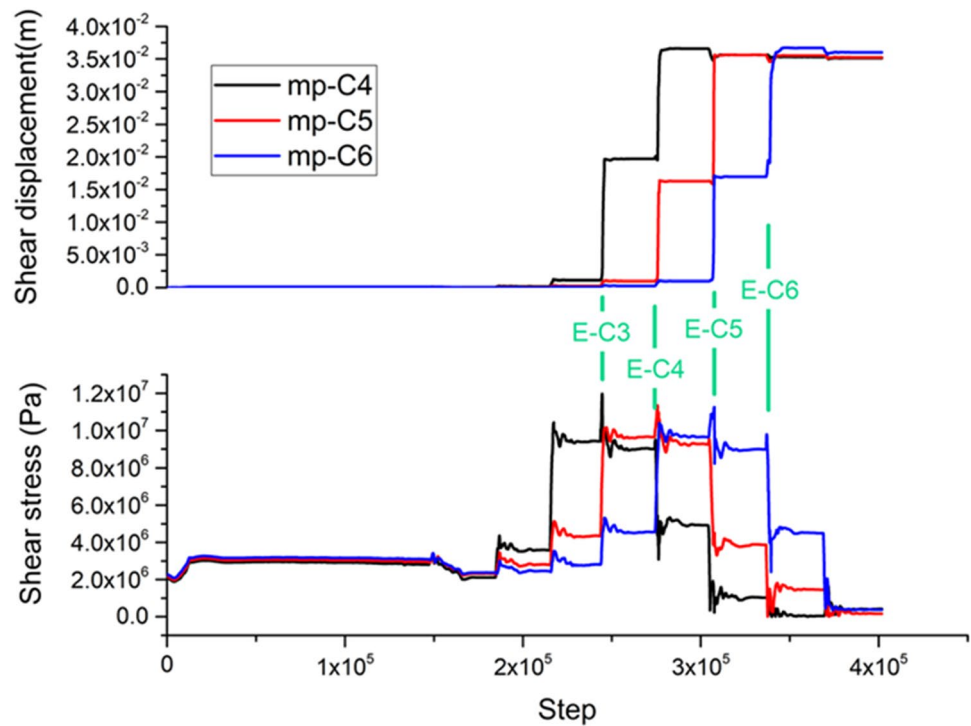

Fig. 5 The evolution of **a** shear displacement and **b** shear stress with excavations of block layers at a series of monitoring points in group A

Fig. 6 The evolution of **a** shear displacement and **b** shear stress with excavations of block layers at a series of monitoring points in group C

Fig. 7 The evolution of **a** shear displacement and **b** shear stress with excavations of block layers at a series of monitoring points in group E
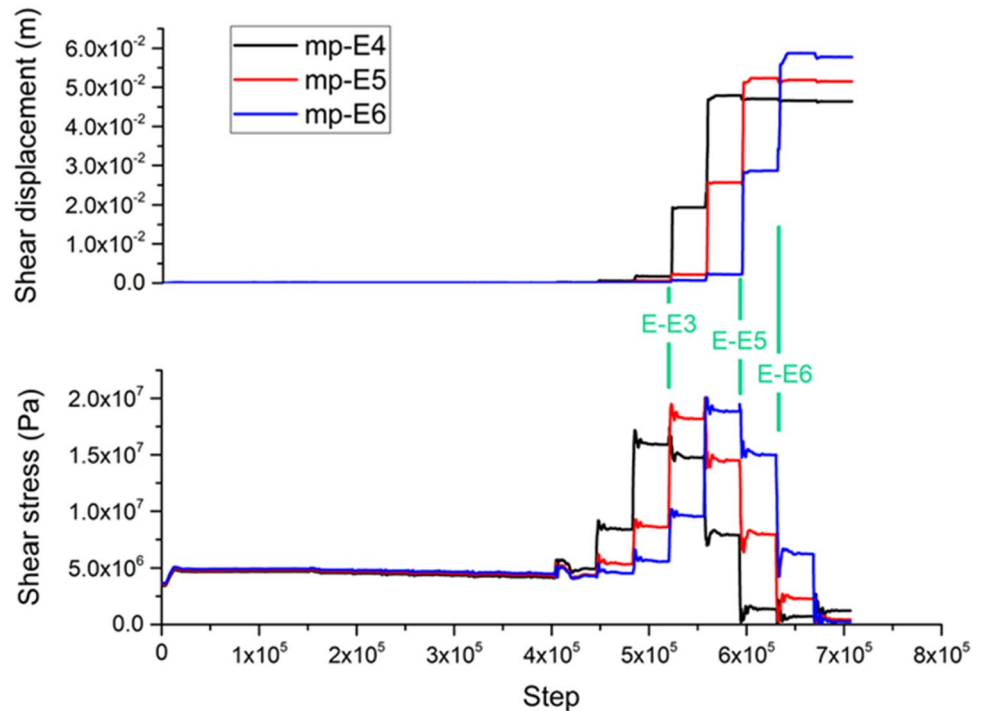

point mp-E5. Regarding the monitoring point mp-E6, the first appearance of shear displacement increase and shear stress drop follow the excavation of block E5. Then, the excavation of block E6 leads to the second shear displacement increase and shear stress decrease at this monitoring point. Compared with the effects exerted by the excavation

of block E5, the removal of the next level of depth, the block E6, yields the same amount of magnitude change of shear stress and a fairly larger shear displacement.

We examine the 4th block layer in the subdivided groups, including block group A, block group C, and block group E, and compare the monitoring points across them (Fig. 8).

Fig. 8 Comparison of the shear displacement and shear stress evolution across monitoring points from group A, group C, and group E
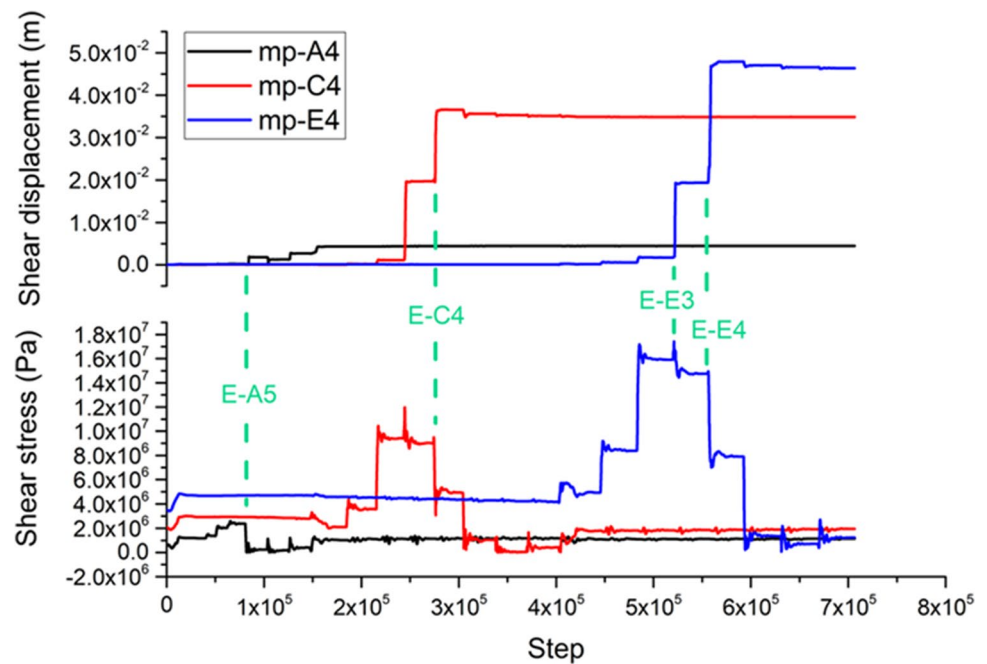
Through the comparison across these groups, we notice that the magnitude of shear displacement and shear stress significantly increase at a greater depth. Meanwhile, the change of shear stress and shear displacement caused by unstable shear slip is more pronounced at deeper depths. When the excavated blocks are distant, the shear stress and shear displacement at these monitoring points slightly fluctuate and tend to be stable as the excavated blocks are located beyond a certain range. According to this comparison across monitoring points from different block groups, it is more clearly shown that the excavated block C4 causes the initial unstable shear slip behavior at mp-C4, which is the monitoring point at the same depth as block C4. Similarly, the monitoring point mp-E4 from the deeper block group experiences the unstable shear slip as early as the excavation of its corresponding block, block E4. In contrast, it is found that the shear slip behavior at monitoring point mp-A4 is caused by the excavation of a deeper block, block A5.

3.3 Seismic Energy Computation and Comparison

The seismic energy change that each subcontact possesses is calculated using the output results of stress and displacement change. By adding seismic energy from all subcontacts, we calculate the seismic energy change arising from the excavation of blocks. To be consistent with the previous analysis of unstable shear slip, we examine the same blocks including A4, C4, and E4. It is found that the seismic energy change mainly concentrates on the region that experiences the excavation of blocks. For example, after the excavation of block A4, a belt shape region appears to be with significantly high

seismic energy, which is located on the identical location of block A4, and is identified on the major joint (Fig. 9a). By continuing to examine the seismic energy distribution after the excavation of block C4, we observe that the high seismic energy zone shifts to the location of the excavation and the seismic energy is significantly higher than that from the excavation of block A4. We further examine the seismic energy distribution after the excavation of E4, which belongs to the group at the deeper depth. It is found that the zone of high seismic energy migrates along the major joint to the location of block E4. Note that the seismic energy change caused by the excavation of block E4 is the largest among these three cases by comparing them. According to the zoom-in view focusing on target blocks, it shows that subcontacts located around middle-level positions of block C4 and block E4 possess relatively higher seismic energy than the peripheral ones. However, the subcontacts generated with the maximum seismic energy in block A4 appear to locate on the very right side (Fig. 9b).

3.4 Seismic Moment Computation and Comparison

We continue to investigate the seismic moment triggered by block excavations along with the unstable shear slip behavior of the major joint (Fig. 10a). According to qualitative analysis and comparison on the same blocks used in previous analyses, the same pattern that a deeper excavation causes larger seismic moment is found and summarized. The seismic moment distribution delineates the shape of excavated blocks as well. In addition, we examine the seismic moment distribution on the zoom-in view

Fig. 9 Seismic energy distribution with block layer excavations in different levels. The left column represents the joint between the hanging wall and the footwall, which is shown in Fig. 4; the right column is the zoom-in view and the front view of the left column
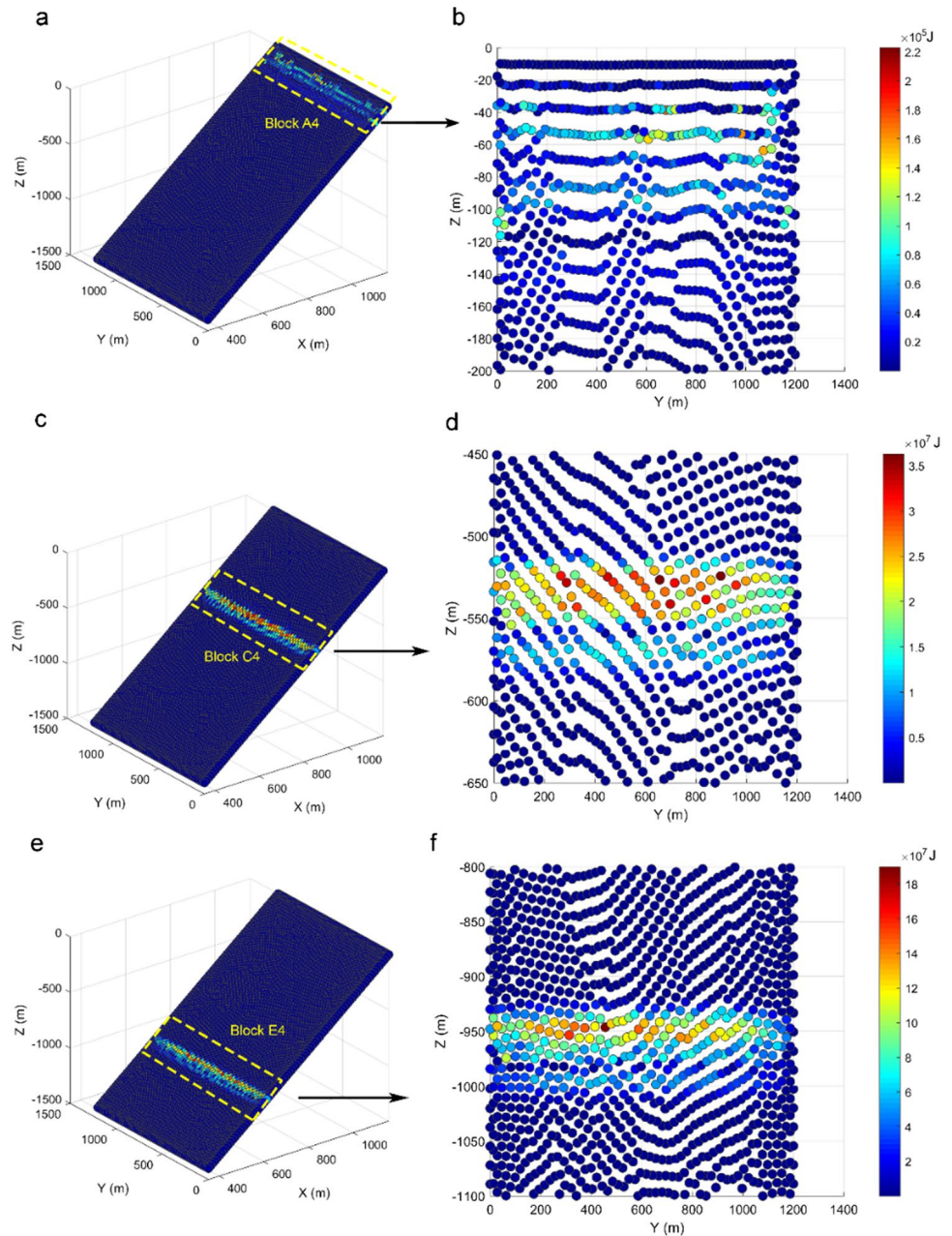
(Fig. 10b) and recognize that the seismic moment of subcontacts is higher in the center than in the periphery of the surrounding joint.

4 Discussion

The distribution of change of seismic moment and seismic energy change, as measured by the difference of subcontacts between statuses that correspond to sequential excavations, implies that mining excavations notably alter the geomechanical conditions and are likely to cause shear slips along discontinuities as well as seismic hazards. The existing discontinuities in

Kiirunavaara Mine significantly undermine the stability of rock masses and amplify the shear slip potential caused by stress perturbations from mining operations. It has been proven that the footwall-parallel fault greatly affects the stability of nearby rock masses, which are especially prone to initiate the motion of shear slip associated with triggering seismic events. Seismic events occurring adjacent to the major discontinuity provide important messages to identify these shear slip behaviors. The DEM numerical modeling is validated so that it can be used to simulate these shear slip behaviors and manifest the signature of shear stress drop and shear displacement increase.

By combining what we know about influences on rock masses stability exerted by existing discontinuities in

Fig. 10 Seismic moment distribution with block layer excavations in different levels
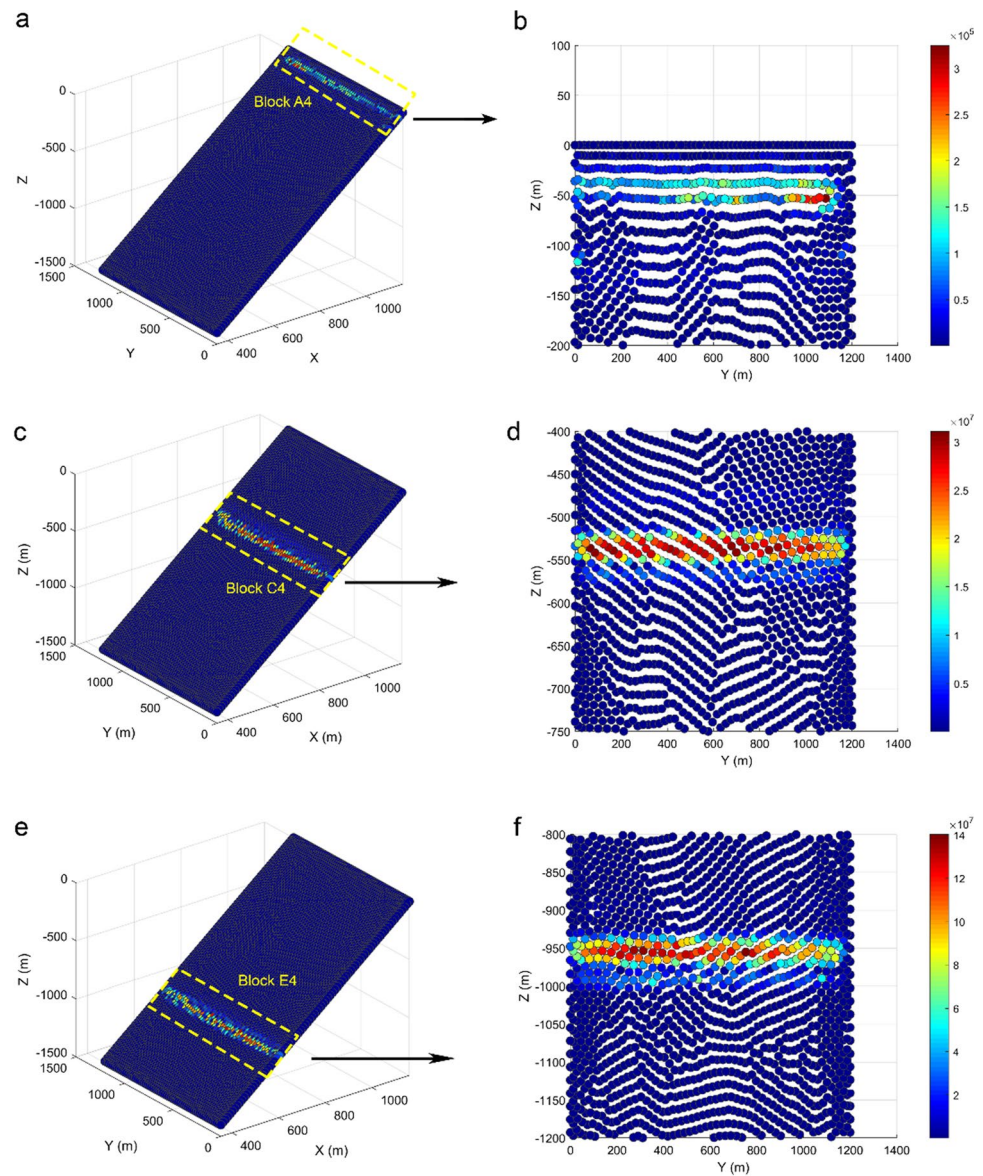
Kiirunavaara Mine, we can identify potential shear ruptures along the weakness plane of the discontinuities. It should be noted that a lot of asperities exist in naturally contacting rocks, and this property plays a role in determining the magnitude and stress drop path along an unstable plane of weakness [20].

Calibration and back analysis using seismic events that are induced during fault slip in underground mines are beneficial to characterize and quantify the stress drop on planes of weakness. As suggested in a previous study, the unstable plane of weakness experiences a stress drop ranging from 5 to 10 MPa and a shear stress decrease of about 20 MPa in an unstable rupture [27]. Furthermore, studies from seismology suggest considering the dynamic friction τ_d, which is defined as a slightly lower level of frictional resistance compared with static friction. The dynamic friction needs to

be considered when slip has been imitated to mobilize. In the scenario of dynamic friction, cohesion is still considered as nearly 0. The stress drop, summarized using mining seismicity data, is found to range from 0.1 to 10 MPa [35], and lab testing data indicate that the stress drop is approximately 5 to 10% [36]. In addition, we compare the seismic moment and seismic energy of four seismic events in Kiirunavaara Mine (Table 1) with the seismic moment and seismic energy caused by excavating Block E4 in modeling results since these events located nearly in the same depth of Block E4. We compute that the total seismic energy is 1.86×10^{10} J and the seismic moment is 7.39×10^{10} N·m by excavating Block E4. According to the four seismic events in situ seismic data survey, the total seismic energy for four seismic event is 4.84×10^7 J. An explanation for this phenomenon is that only a portion of released seismic energy turns into

forming these major seismic events. The rest seismic energy contributes to frictional loss and microseismicity. The average seismic moment is 1.15×10^{12} Nm from the seismic survey, indicating that the DEM modeling underestimates the seismic moment. This underestimation might be because the modeling cannot capture the dynamic ruptures during shear slip. Instead, the seismic moment is calculated using relative locations of subcontacts between the status before the shear slip and after the shear slip.

We confirmed that when rigidity increases, relative displacement may reduce to the point that slip is stable. We performed the effects of roughness parameters and rigidity of the rock on the CY post-peak behavior (Supplementary material). Figure 11 shows that when the rigidity increases, the loading system is more stable. The relative displacement reduces to a point that the slip is stable. Comparing Fig. S7 and Fig. 11, it can be inferred that the slip energy increases with the increase rigidity of the rock increases. Additionally, when the rigidity increases, the preexisting sudden increase of the shear displacement and the sudden drop of the stress will disappear. The shear slip, accordingly, turns into stable.

In the early mining history of the Kiirunavaara Mine, geohazards mainly came from gravity falls in the drifts. However, the major concern of the overall stability nowadays is surrounding the highly stressed regions at great depth and mining-induced seismic events including the fault slip type and the strain burst type. Mining operations such as production blasts and excavations significantly alter the regional stress field due to the heterogeneities and geological structures within the rock mass, therefore activating joints and faults to result in seismic active structures. There is still uncertainty in triggering seismic events. Then mines will be better able to respond to unanticipated threats of rock mass failures in terms of shear rupture and seismic hazards. Because characterizing geological discontinuities and incorporating them in numerical modeling, as a way to better take advantage of this information, set the stage for quantitatively examining fault interactions with mining, it will always be seen as an essential capacity for sustaining the rock mass safety of mines.

It is noteworthy to know that shear rupture barely occurs along regular shape planes in reality, and therefore, the rupture areas are neither circular nor rectangular as hypothesized in most studies. Faults that exist in nature contain jogs, steps, branching, and splays extending to all directions [2]. Smooth ruptures, accordingly, are seldom due to the complexity of fault structures. Instead, rough features are recognized in the contacting surfaces of faults, leading to unanticipated behaviors such as heterogeneous dynamic ruptures and sudden rupture halting other than ideal shear ruptures as hypothesized. Therefore, to avoid underestimating the influences from
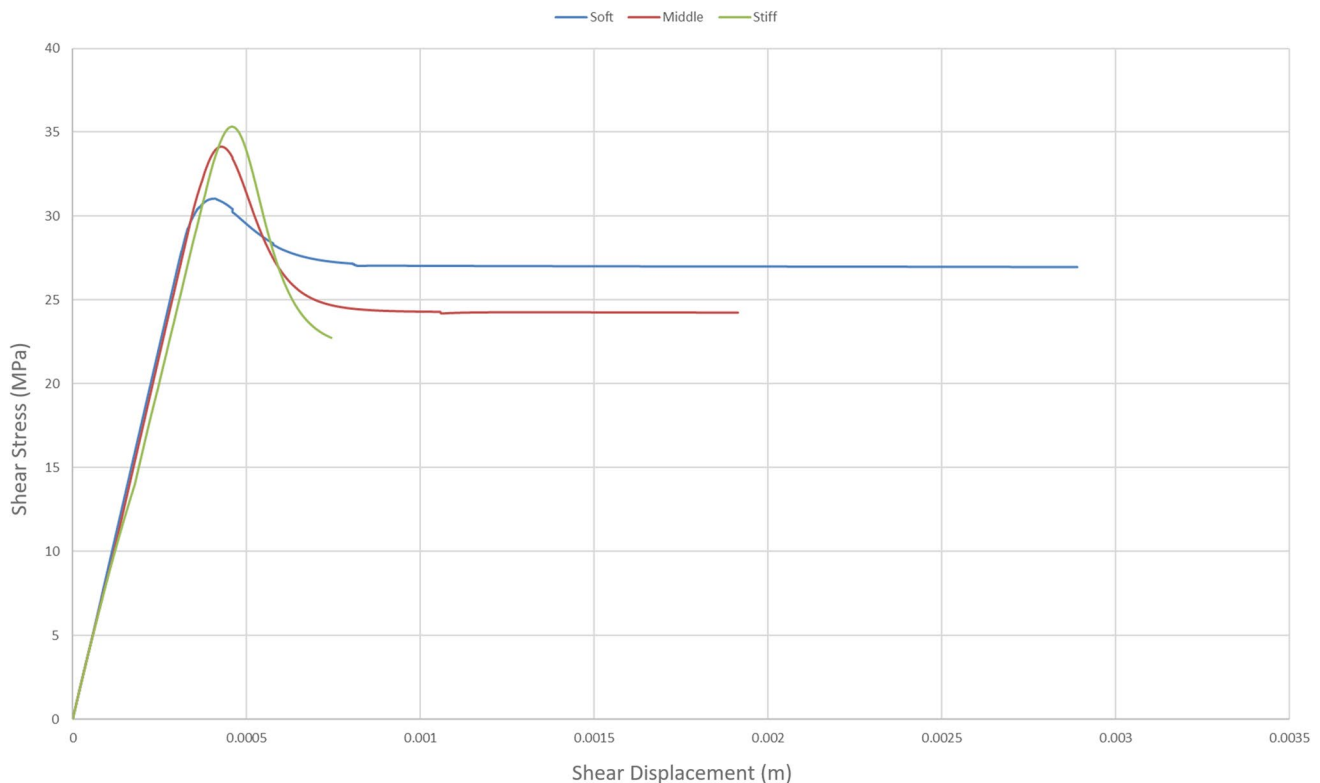
Fig. 11 The relationship between the shear stress and the shear displacement for loading systems with different rigidity

heterogeneous structures of fault, it is particularly important that the assessment of seismic moment and seismic energy release can consider and incorporate the effects of the complexity of real faults.

5 Conclusions

Discontinuities in rock masses significantly affect the geomechancial responses of rock masses during mining operations. Excavations of the orebody are likely to cause shear slip along the discontinuities, which experience abrupt shear displacement increase and sudden shear stress drop. DEM modeling facilitates quantifying variations of the seismic moment and seismic energy arising from the shear slip along the plane of discontinuities. Accurate and fast quantification for a seismic moment and seismic energy change during shear slip can help better predict seismic hazards caused by fault slip due to the existence of discontinuities and perturbations from mining operations.

We apply the numerical models of 3DEC to emulate the major geological structures with mining operations and characterize seismic potential. We computed the seismic energy and seismic moment using the numerical modeling method and the analytic method. We compared the result of summing seismic energy and seismic moment from the subcontacts of numerical models and the result of the analytic method and validated the reliability of the numerical models. The 3DEC model can efficiently reflect the shear slip signature along discontinuities by adapting subcontacts in mesh networks. The seismic energy and seismic moment analysis still need to be further studied with in situ measurements in mining fields.

References

1. Cook NGW (1976) Seismicity associated with mining. Eng Geol 10(2–4):99–122. https://doi.org/10.1016/0013-7952(76)90015-6

2. Bormann P, Di Giacomo D (2011) The moment magnitude M w and the energy magnitude M_e: common roots and differences. J Seismolog 15(2):411–427

3. Bürgmann R, Pollard DD, Martel SJ (1994) Slip distributions on faults: effects of stress gradients, inelastic deformation, heterogeneous host-rock stiffness, and fault interaction. J Struct Geol 16(12):1675–1690. https://doi.org/10.1016/0191-8141(94)90134-1

4. Eremin M, Esterhuizen G, Smolin I (2020) Numerical simulation of roof cavings in several Kuzbass mines using finite-difference continuum damage mechanics approach. Int J Min Sci Technol 30(2):157–166. https://doi.org/10.1016/j.ijmst.2020.01.006

5. Malan DF (1999) Time-dependent behaviour of deep level tabular excavations in hard rock. Rock Mech Rock Eng 32(2):123–155

6. McGarr A, Green RWE (1975) Measurement of tilt in a deep-level gold mine and its relationship to mining and seismicity. Geophys J Int 43(2):327–345

7. Elmo D, Stead D, Eberhardt E, Vyazmensky A (2013) Applications of finite/discrete element modeling to rock engineering problems. Int J Geomech 13(5):565–580. https://doi.org/10.1061/(ASCE)GM.1943-5622.0000238

8. Vyazmensky A, Stead D, Elmo D, Moss A (2010) Numerical analysis of block caving-induced instability in large open pit slopes: a finite element/discrete element approach. Rock Mech Rock Eng 43(1):21–39

9. Xu N, Zhang J, Tian H, Mei G, Ge Q (2016) Discrete element modeling of strata and surface movement induced by mining under open-pit final slope. Int J Rock Mech Min Sci 88:61–76

10. Boltz MS (2014) Mining-induced seismicity and FLAC3D Modeling at the Trail Mountain Mine. Master dissertation. The University of Utah. https://scholar.google.com/scholar_lookup?title=Mining-Induced%20Seismicity%20and%20FLAC3D%20Modeling%20at%20the%20Trail%20Mountain%20Mine&publication_year=2014&author=M.S.%20Boltz

11. Mercer RA, Bawden WF (2005) A statistical approach for the integrated analysis of mine-induced seismicity and numerical stress estimates, a case study—part I: developing the relations. Int J Rock Mech Min Sci 42(1):47–72. https://doi.org/10.1016/j.ijrmms.2004.07.006

12. Heunis R (1980) The development of rock-burst control strategies for South African gold mines. J South Afr Inst Min Metall 80(4):139–150

13. Fritschen R (2010) Mining-induced seismicity in the Saarland, Germany. Pure appl geophys 167(1):77–89. https://doi.org/10.1007/s00024-009-0002-7

14. Iannacchione AT, Tadolini SC (2016) Occurrence, predication, and control of coal burst events in the US. Int J Min Sci Technol 26(1):39–46. https://doi.org/10.1016/j.ijmst.2015.11.008

15. Maxwell SC, Young RP (1992) Sequential velocity imaging and microseismic monitoring of mining-induced stress change. Pure Appl Geophys 139(3):421–447. https://doi.org/10.1007/BF008 79945

16. Sainoki A, Mitri HS (2014) Dynamic behaviour of mining-induced fault slip. Int J Rock Mech Min Sci 66:19–29. https://doi.org/10.1016/j.ijrmms.2013.12.003

17. Orlecka-Sikora B, Papadimitriou EE, Kwiatek G (2009) A study of the interaction among mining-induced seismic events in the Legnica-Głogów Copper District, Poland. Acta Geophysica 57(2):413–434. https://doi.org/10.2478/s11600-008-0085-z

18. Barton N (1973) Review of a new shear-strength criterion for rock joints. Eng Geol 7(4):287–332. https://doi.org/10.1016/0013-7952(73)90013-6

19. Meng F, Zhou H, Li S, Zhang C, Wang Z, Kong L, Zhang L (2016) Shear behaviour and acoustic emission characteristics of different joints under various stress levels. Rock Mech Rock Eng 49(12):4919–4928. https://doi.org/10.1007/s00603-016-1034-9

20. Ryder JA (1988) Excess shear stress in the assessment of geologically hazardous situations. J South Afr Inst Min Metall 88(1):27–39

21. Sleep NH, Blanpied ML (1992) Creep, compaction and the weak rheology of major faults. Nature 359(6397):687–692

22. Xu YH, Cai M (2017) Influence of loading system stiffness on post-peak stress–strain curve of stable rock failures. Rock Mech Rock Eng 50(9):2255–2275. https://doi.org/10.1007/s00603-017-1231-1

23. Zhang F, Liu G, Chen W, Liang S, Chen R, Han W (2012) Human-induced landslide on a high cut slope: a case of repeated failures due to multi-excavation. J Rock Mech Geotech Eng 4(4):367–374. https://doi.org/10.3724/sp.j.1235.2012.00367

24. Swanson MT (1992) Fault structure, wear mechanisms and rupture processes in pseudotachylyte generation. Tectonophysics 204(3–4):223–242. https://doi.org/10.1016/0040-1951(92)90309-T

25. Brune JN (1970) Tectonic stress and the spectra of seismic shear waves from earthquakes. J Geophys Res 75(26):4997–5009. https://doi.org/10.1029/JB075i026p04997

26. Simpson DW (1986) Triggered earthquakes. Annu Rev Earth Planet Sci 14:21

27. Gu R, Ozbay U (2015) Numerical investigation of unstable rock failure in underground mining condition. Comput Geotech 63:171–182

28. Gu R, Ozbay U (2014) Distinct element analysis of unstable shear failure of rock discontinuities in underground mining conditions. Int J Rock Mech Min Sci 68:44–54

29. Zoheir K, Ozbay U (2018) Computational framework for simulating rock burst in shear and compression. Int J Rock Mech Min Sci 110:279–290

30. Hamdi P, Stead D, Elmo D, Töyrä J (2018) Use of an integrated finite/discrete element method-discrete fracture network approach to characterize surface subsidence associated with sub-level caving. Int J Rock Mech Min Sci 103:55–67

31. Dahnér C, Malmgren L, Boškovic M (2012) Transition from non-seismic mine to a seismically active mine: Kiirunavaara Mine. ISRM International Symposium-EUROCK 2012. OnePetro. https://scholar.google.com/scholar?hl=en&as_sdt=0%2C5&q=transiation+from+non-seismic+mine+to+a+seismically+active+mine%3A+Kiirunavaara&btnG=

32. Cundall PA, Hart RD (1992) Numerical modelling of discontinua. Eng Comput 9:101–13. https://scholar.google.com/scholar?hl=en&as_sdt=0%2C5&q=Cundall+PA%2C+Hart+RD+%281992%29+Numerical+modelling+of+discontinua.+Eng+Comput.+9%3A101%E2%80%9313&btnG=

33. Lemos, JV, Cundall PA, Dasgupta B (1997) Earthquake analysis of concrete gravity dams on jointed rock foundations. Proc., 2nd Int. Conf., Dam Safety Evaluation, Balkema, Rotterdam, The Netherlands, pp 339–350. https://scholar.google.com/scholar?hl=en&as_sdt=0%2C5&q=Lemos%2C+JV%2C+Cundall%2C+PA%2C+and+Dasgupta%2C+B+%281997%29+Earthquake+analysis+of+concrete+gravity+dams+on+jointed+rock+foundations.+Proc.%2C+2nd+Int.+Conf.%2C+Dam+Safety+Evaluation&btnG=

34. Kanamori H (1977) The energy release in great earthquakes. J Geophys Res 82(20):2981–2987

35. Yamada T, Mori JJ, Ide S, Abercrombie RE, Kawakata H, Nakatani M, Lio Y, Ogasawara H (2007) Stress drops and radiated seismic energies of microearthquakes in a South African gold mine. J Geophys Res 112(B03305). https://doi.org/10.1029/2006JB004553; https://scholar.google.com/scholar?hl=en&as_sdt=0%2C5&q=Stress+drops+and+radiated+seismic+energies+of+microearthquakes+in+a+South+African+gold+mine&btnG=

36. Leeman JR, Marone C, Saffer DM (2018) Frictional mechanics of slow earthquakes. J Geophys Res: Solid Earth 123(9):7931–7949